Environmental Science Processes & Impacts



PAPER



Cite this: *Environ. Sci.: Processes Impacts*, 2016, **18**, 1078

# Wildfires and water chemistry: effect of metals associated with wood ash†

José M. Cerrato,*[a] Johanna M. Blake,‡[b] Chris Hirani,[c] Alexander L. Clark,[d] Abdul-Mehdi S. Ali,[e] Kateryna Artyushkova,[f] Eric Peterson[f] and Rebecca J. Bixby[d]

The reactivity of metals associated with ash from wood collected from the Valles Caldera National Preserve, Jemez Mountains, New Mexico, was assessed through a series of laboratory experiments. Microscopy, spectroscopy, diffraction, and aqueous chemistry measurements were integrated to determine the chemical composition of wood ash and its effect on water chemistry. Climate change has caused dramatic impacts and stresses that have resulted in large-scale increases in wildfire activity in semi-arid areas of the world. Metals and other constituents associated with wildfire ash can be transported by storm event runoff and negatively affect the water quality in streams and rivers. Differences among ash from six tree species based on total concentrations of metals such as Ca, Al, Mg, Fe, and Mn were identified using non-metric multidimensional analysis. Metal-bearing carbonate and oxide phases were quantified by X-ray diffraction analyses and X-ray spectroscopy analyses. These metal-bearing carbonate phases were readily dissolved in the first 30 minutes of reaction with 18 MΩ water and 10 mM $HCO_3^-$ in laboratory batch experiments which resulted in the release of metals and carbonates in the ash, causing water alkalinity to increase. However, metal concentrations decreased over the course of the experiment, suggesting that metals re-adsorb to ash. Our results suggest that the dissolution of metal-bearing carbonate and oxide phases in ash and metal re-adsorption to ash are relevant processes affecting water chemistry after wildfire events. These results have important implications to better understand the impact of wildfire events on water quality.

Received 1st March 2016
Accepted 7th July 2016

DOI: 10.1039/c6em00123h

rsc.li/process-impacts

### Environmental impact

Metals associated with wildfire ash can be transported after post-fire storm events and affect surface water chemistry. Differences in the chemical composition and structure in wood ash from various tree species collected from the Valles Caldera National Preserve in New Mexico were identified in experiments conducted under controlled laboratory conditions. Metal-bearing carbonate and oxide phases in wood ash can readily dissolve in water and cause an initial increase in metal concentrations and alkalinity. However, wood ash reactivity over time can cause pH fluctuations in low alkalinity waters and result in metal re-adsorption. These results have important implications to better understand the impact of metals associated with wood ash on water chemistry.

## 1. Introduction

Wildfires catastrophically affect natural resources, causing profound societal and economic impacts. These events are particularly relevant in semi-arid areas of the world facing severe challenges of water scarcity. For instance, the forests of the western United States have suffered from large-scale increases in wildfire severity.[1–3] The combination of early spring snowmelt,[4] decreased winter precipitation,[5] and greater vapor-pressure deficit in the warm season[6] results in substantial water limitation stress on western United States forests.[7] Additionally, increased drought severity and frequency related to climate change has become a concern in the southwestern United States.[8] These complex interactions, combined with uncontrolled human development and forest management (*i.e.* 100 years of fire suppression) drive wildfire activity, resulting in

[a]Department of Civil Engineering, MSC01 1070, University of New Mexico, Albuquerque, New Mexico 87131, USA. E-mail: jcerrato@unm.edu; Fax: +1 505 277 1918; Tel: +1 505 277 0870

[b]Department of Chemistry, MSC03 2060, University of New Mexico, Albuquerque, New Mexico 87131, USA

[c]Department of Chemical and Biological Engineering, MSC01 1120, University of New Mexico, Albuquerque, New Mexico 87131, USA

[d]Department of Biology and Museum of Southwestern Biology, MSC03 2020, University of New Mexico, Albuquerque, New Mexico 87131, USA

[e]Department of Earth and Planetary Sciences, MSC03 2040, University of New Mexico, Albuquerque, New Mexico 87131, USA

[f]Department of Chemical and Biological Engineering and Center for Microengineered Materials, University of New Mexico, MSC 01 1120, Albuquerque, New Mexico 87131, USA

† Electronic supplementary information (ESI) available. See DOI: 10.1039/c6em00123h

‡ Current address: U.S. Geological Survey, New Mexico Water Science Center, 5338 Montgomery Blvd., Albuquerque, New Mexico, USA.

 

negative effects on the quality, transport, and ecosystem linkages of lotic waters.[9]

The catastrophic effects caused by the Las Conchas Fire in New Mexico in 2011 served as a motivation for this study. The Las Conchas Fire, one of the largest forest fires in the recorded history of New Mexico, burned over 63 000 hectares (156 000 acres) of the Jemez Mountains, which are an important headwater source for the Middle Rio Grande Valley.[10] Additionally, this event impacted over 34% of the Valles Caldera National Preserve (VCNP).[11] In 2013, the Thompson Ridge fire burned an additional 23 965 acres in the VCNP. The areas with high burn severity from each of these fires occurred near the headwaters of multiple streams within the caldera including the East Fork Jemez River (Fig. 1). This fire had devastating impacts on downstream communities such as significant erosion of the burn scar, and the closure of drinking water treatment facilities for the cities of Albuquerque and Santa Fe due to the high turbidity of the water following storm events that created large debris flows.[12] Extensive quantities of ash produced from the Las Conchas wildfire flowed through smaller tributaries and into important drinking water sources.[13] Significant sags in the dissolved oxygen (DO) concentrations and pH level decreases were observed throughout the Rio Grande continuum, while turbidity spikes increased to levels above 1000 NTU.[13,14] Dissolved concentrations of nitrate (six times higher than background) and phosphate (100 times higher than background) in the East Fork Jemez River increased after monsoonal events following the Las Conchas Fire.[15] Storm event runoff, such as the one that the Rio Grande experienced after the Las Conchas fire, can mobilize organic matter, metals, and nutrients associated with ash into streams and rivers downstream of the burned areas.

While research has been conducted to better understand the effect of catastrophic events, such as the Las Conchas fire, on water quantity and quality,[13,15] limited studies have focused on investigating the effect of trace metals contained in wildfire ash.[16–18] It is likely that both biological and chemical factors have an effect on decreasing pH and dissolved oxygen concentrations as suggested in a previous study.[13] A critical knowledge gap exists related to the fundamental chemical and biological mechanisms that affect metal deposition/release from ash and how these could potentially impact water sources after wildfire events.

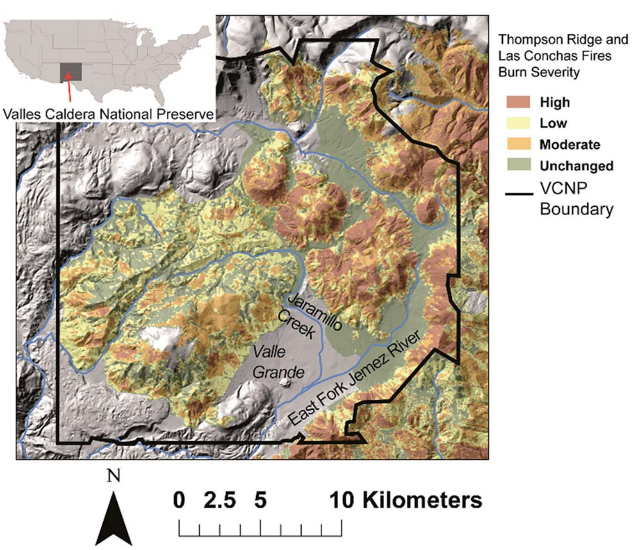


Fig. 1 Site map of the Valles Caldera National Preserve, New Mexico.

The specific processes controlling the magnitude and persistence of metals post-fire remain unknown.[19] Concentrations of metals, such as copper (Cu), cadmium (Cd), zinc (Zn), and lead (Pb), have been measured up to three orders of magnitude higher in burned catchments compared with unburned natural areas after storm events following catastrophic wildfires in southern California.[19–21] A study conducted after the Cerro Grande fire in 2000 in New Mexico reported that metals in unfiltered runoff were mostly associated with the particulate fraction and not detected in the dissolved water fraction.[22] Furthermore, the water soluble behavior of calcium (Ca), magnesium (Mg), and potassium (K) was reported in an investigation of ash collected in Portugal which also noticed an increase in water pH and carbonate ($CO_3^{2-}$) concentration with fire severity.[17] The presence of increased inorganic carbon in water post-fire is due to the interfacial interaction of water and minerals that compose wood ash. For instance, carbonates, silicates, oxides, phosphates, sulfates, and amorphous phases are either present as primary minerals in plant materials or undergo structural alterations from the heating during combustion.[23–26] Obtaining representative ash samples after storm events post-fire is a major challenge due to variations in ash and soil composition, particle size, and thickness of ash layers transported by runoff.[27] Although ash from wildfires can differ quantitatively from laboratory ash samples, previous studies have found common features between field and laboratory ash samples that could be beneficial to investigate relevant processes under controlled conditions.[26,27]

The objective of this study is to investigate under controlled laboratory conditions the effect of metals associated with ash on water chemistry by integrating solution chemistry measurements with spectroscopy, microscopy, and X-ray diffraction. Ash from trees collected from the VCNP, New Mexico, was used in this investigation. The present study intends to improve our understanding of key chemical processes affecting water quality which are relevant to post-wildfire events.

## 2. Materials and methods

### 2.1. Materials

Wood was collected from six tree species [Ponderosa Pine (*Pinus scopulorum*), Colorado blue spruce (*Picea pungens*), Gambel Oak (*Quercus gambelii*), Douglas Fir (*Pseudotsuga menziesii* var. *glauca*), one-seeded juniper (*Juniperus monosperma*), and quaking aspen (*Populus tremuloides*)] from the VCNP, focusing on taxa present in areas that have been affected by the Las Conchas and other wildfires in the past. Soil samples were also obtained from the same locations where pine, aspen, and spruce were collected. These tree and soil samples were collected at the following corresponding latitudes and longitudes: pine (35° 51′ 43.3″, 106° 36′ 07.7″), aspen (35° 54′ 32.5″, 106° 36′ 59.0″), spruce (35° 52′ 22.0″, 106° 37′ 19.0″), fir (35° 52′ 21.6″, 106° 37′ 18.3″), juniper (35° 51′ 40.4″, 106° 36′ 12.1″), and oak (35° 52′ 07.5″, 106° 36′ 59.0″). Ash was produced from whole branches in the laboratory by burning wood from the six tree species in a muffle furnace at 550 °C for 4 hours. This temperature and time were chosen to represent fire severity and burn intensity conditions that would lead to considerable heat release over time to produce organic matter loss as reported in catastrophic events.[28,29]

### 2.2. Solid characterization

Solid phase analyses were performed on wood ash samples applying X-ray photoelectron spectroscopy (XPS), scanning electron microscopy coupled to energy dispersive X-ray spectroscopy (SEM/EDX), X-ray diffraction (XRD), and X-ray fluorescence (XRF). Additionally, XRD analyses were performed on selected soil samples from the Valles Caldera National Preserve (VCNP). A Kratos AXIS-Ultra DLD X-ray Photoelectron Spectrometer (XPS) was used to acquire the near surface (5–10 nm) elemental composition and oxidation states. Gold powder was deposited on each sample, and Au 4f spectra were acquired for calibration purposes. All the spectra were charge referenced to Au 4f at 84 eV and processing was done using CasaXPS. A 70% Gaussian/30% Lorentzian (GL (30)) line shape was used for the curve-fits. Ash samples were analyzed using a JEOL 5800 scanning electron microscope (SEM) equipped with an Oxford (Link) Isis energy dispersive X-ray analyzer (EDX). We also used the Rigaku Smart Lab X-ray diffractometer (XRD), using Cu K$\alpha$ radiation with a scintillation detector and a graphite monochromator, to obtain information on the crystallinity, mineral structure, and normalized approximate percentage amount of mineral phases present in the ash samples. The XRD data were analyzed using Jade® software. Measurements of X-ray fluorescence (XRF) were conducted to determine bulk elemental composition using an EDAX Orbis with a Rh tube source and a titanium adsorption edge filter. Samples were measured in a vacuum with a filament voltage of 20 kV and a current of 15 μA.

### 2.3. Laboratory experiments

Ash samples were digested in triplicate ($n = 3$) for near-total elemental cation analysis using aqua regia [2 mL nitric acid ($HNO_3$, 67–70% by mass, trace metal grade) and 6 mL hydrochloric acid (HCl, 34–37% by mass, trace metal grade), 4 hour reaction at 95 °C]. Ash samples were also extracted in triplicate with 18 MΩ water for anion analysis (2 hour reaction).

Batch reactors were operated in triplicate by reacting 3 g of ash per liter of 18 MΩ water and a 10 mM $NaHCO_3$ solution. For the first experiment, each replicate was sampled at 0, 1, 2, 4, 24, 48, and 72 hours. The replicates were mixed continuously during the experiment in closed centrifuge tubes. At each time point, the pH was measured and aliquots of samples were collected for both cation [aluminium (Al), calcium (Ca), iron (Fe), potassium (K), magnesium (Mg), manganese (Mn), nickel (Ni), vanadium (V), lead (Pb), copper (Cu), and zinc (Zn)] and anion [fluoride ($F^-$), chloride ($Cl^-$), bromide ($Br^-$), nitrite ($NO_2^-$), nitrate ($NO_3^-$), phosphate ($PO_4^{3-}$), and sulfate ($SO_4^{2-}$)] analyses. In an additional experiment, the samples were prepared at 3 g ash per L concentrations in 300 mL ashed biochemical oxygen demand (BOD) bottles. The replicates were sampled for alkalinity and dissolved organic carbon (DOC) at 1, 24, and 72 hours.

### 2.4. Solution chemistry analyses

Aqueous chemistry analyses were performed using inductively coupled plasma-optical emission spectroscopy (ICP-OES) (Perkin Elmer Optima 5300 DV) for Ca, Mg, Al, Fe, Mn, Pb, Zn, Cu, Ni, and V; and inductively coupled plasma-mass spectrometry (ICP-MS) (Perkin Elmer NexION 300D-Dynamic Reaction Cell) for Pb, Zn, Cu, Ni, and V in aqueous solutions in which metals were present at concentrations lower than the ICP-OES detection limit. The detection limits for these instruments are provided in the ESI (Table S1†). These ICP-OES and ICP-MS (indium was used as the internal standard) were calibrated with a 5-point calibration curve and quality assurance and quality control measures were taken to ensure the quality of the results. Ion chromatography (ThermoFisher ICS-1100) was used for anion analyses (*e.g.*, $F^-$, $Cl^-$, $Br^-$, $NO_2^-$, $NO_3^-$, $PO_4^{3-}$, and $SO_4^{2-}$). The DOC samples were measured using a Shimadzu TOC-5050A. The samples were acidified using 6 N HCl and then measured using the method for non-purgeable organic carbon. Alkalinity was measured by colorimetric titration, using 0.02 N sulfuric acid as the titrant and bromocresol green/methyl red as the indicators for total alkalinity.[30]

### 2.5. Statistical analyses

Total elemental and anion concentrations from the initial aqueous chemistry analysis were evaluated using the vegan package in PC-ORD.[31] The data were examined using non-metric multidimensional scaling (NMDS), a non-parametric multivariate ordination technique, to determine the chemical ash similarities among tree species. Multivariate Curve Resolution (MCR) was used to analyze XRF data. Elemental images were acquired and combined into multispectral dataset for further analysis in Matlab. MCR using a non-negativity option for both spectral and image dimensions was applied to convert a set of original elemental images into distribution maps with the corresponding loadings (weight) of the original images.

## 3. Results and discussion

### 3.1. Near-total elemental composition (anion extraction and cation acid digestions)

The near-total elemental concentrations obtained for soil and ash samples in this study are presented in Table 1. The chemical composition of the soils is similar for all elements. Interestingly, the metal concentrations in ash samples obtained for all tree species is higher than those for soil samples. Differences in total metal concentrations were observed in ash from the tree species considered in this study. For example, major elements such as Ca (mean concentrations range 159 735–219 183 mg kg$^{-1}$) and Mg (mean concentration range 5964–12 949 mg kg$^{-1}$) were predominant in ash from all tree species (Table 1). The transition metals Fe (mean concentrations range 350–6900

 

Table 1 Mean ± standard deviation of the near-total elemental content (mg $kg^{-1}$) from acid digestions with aqua regia ($n$ = 3) for wood ash (from pine, aspen, spruce, fir, juniper, and oak) and soil from locations of tree samples for pine, aspen and spruce

| | Ca | Mg | Al | Fe | Mn | V | Pb | Zn | Cu | Ni |
|---|---|---|---|---|---|---|---|---|---|---|
| **Ash elemental content (mg $kg^{-1}$)** | | | | | | | | | | |
| Pine | 159 735 ± 3743 | 6975 ± 8.13 | 7840 ± 230 | 5910 ± 192 | 2050 ± 72.7 | 57.4 ± 15.9 | 53.2 ± 1.97 | 1381 ± 46.3 | 245 ± 4.19 | 208 ± 0.828 |
| Aspen | 219 183 ± 7413 | 12 949 ± 247 | 507 ± 17.5 | 359 ± 36.1 | 292 ± 12.3 | 89.7 ± 9.71 | 35.1 ± 3.02 | 1955 ± 90.4 | 196 ± 4.00 | 199 ± 1.70 |
| Spruce | 135 353 ± 2266 | 5964 ± 14.8 | 7775 ± 115 | 6959 ± 113 | 6015 ± 108 | 63.4 ± 21.8 | 52.7 ± 7.37 | 815 ± 3.43 | 161 ± 2.46 | 207 ± 0.498 |
| Fir | 193 157 ± 1753 | 7780 ± 2731 | 68 052 ± 51.8 | 5594 ± 81.3 | 4059 ± 49.6 | 71.4 ± 14.1 | 46.0 ± 2.65 | 675 ± 34.6 | 226 ± 2.06 | 205 ± 0.234 |
| Juniper | 209 960 ± 2934 | 12 318 ± 65.8 | 2322 ± 45.8 | 1733 ± 44.0 | 1517 ± 21.5 | 38.3 ± 17.0 | 34.4 ± 3.18 | 301 ± 11.7 | 173 ± 2.21 | 207 ± 0.785 |
| Oak | 197 788 ± 1403 | 8470 ± 3401 | 3486 ± 14.8 | 2799 ± 37.1 | 3274 ± 64.3 | 45.4 ± 15.3 | 44.2 ± 5.58 | 661 ± 17.8 | 233 ± 1.04 | 207 ± 1.18 |
| **Soil elemental content (mg $kg^{-1}$)** | | | | | | | | | | |
| Pine | 2896 ± 131 | 1143 ± 54.2 | 4769 ± 256 | 6995 ± 302 | 449 ± 19.8 | 17.6 ± 1.57 | 5.89 ± 0.237 | 25.5 ± 1.31 | 8.48 ± 0.268 | 1.65 ± 0.188 |
| Aspen | 3576 ± 149 | 862 ± 36.4 | 4545 ± 221 | 13 270 ± 440 | 547 ± 20.1 | 14.9 ± 2.77 | 9.63 ± 0.352 | 51.8 ± 1.09 | 14.4 ± 0.435 | 5.81 ± 0.339 |
| Spruce | 2731 ± 104 | 1510 ± 38.8 | 6064 ± 230 | 8592 ± 283 | 420 ± 15.2 | 11.7 ± 5.44 | 6.83 ± 0.111 | 23.8 ± 1.64 | 10.5 ± 1.46 | 3.90 ± 0.281 |

mg $kg^{-1}$) and Mn (mean concentration range 292–6015 mg $kg^{-1}$), and the metal Zn (mean concentration range 301–1955 mg $kg^{-1}$) were present at higher concentrations than other metals such as Ni (mean concentration range 199–208 mg $kg^{-1}$), Cu (mean concentration range 161–245 mg $kg^{-1}$), V (mean concentration range 38–89 mg $kg^{-1}$), and Pb (mean concentration range 34–53 mg $kg^{-1}$) (Table 1). Anion extraction concentrations are presented in Table S2.† Sulfate has the highest concentrations among all species ranging from 9861–23 478 mg $kg^{-1}$ followed by nitrate, chloride and phosphate. These results are consistent with other studies that reported the predominance of Ca, K, Mg, P, Mn, Fe, and Al in the total elemental concentration of composite ash from both ponderosa pine (*Pinus scopulorum*) and lodgepole pine (*Pinus contorta*).[32,33]

The ordination plot showed a clear separation of ash samples from the six tree species based on total elemental concentrations (20 cations, 7 anions) (Fig. 2). The results indicate that while some species are similar in elemental composition (*e.g.*, aspen, oak, juniper, and spruce), spruce and pine ash samples are different from each other and from other taxa based on their elemental composition. The elements Mn, Fe, and Al were more heavily weighted for spruce and pine but less important in aspen; Mg was more heavily weighted in aspen and juniper ash. While comparative ash chemistry from multiple tree species is not widely reported in the literature, this study supports published data showing that elemental composition can characterize different living tree species.[34]

Based on the aqueous chemistry and NMDS ordination results, three species with the most different elemental compositions (aspen, pine, and spruce) were selected for additional characterization and analysis.

### 3.2. Microscopy and X-ray spectroscopy analyses

The SEM micrographs and EDX spectra (Fig. 3) show differences in form and elemental composition of the ash from pine, aspen,

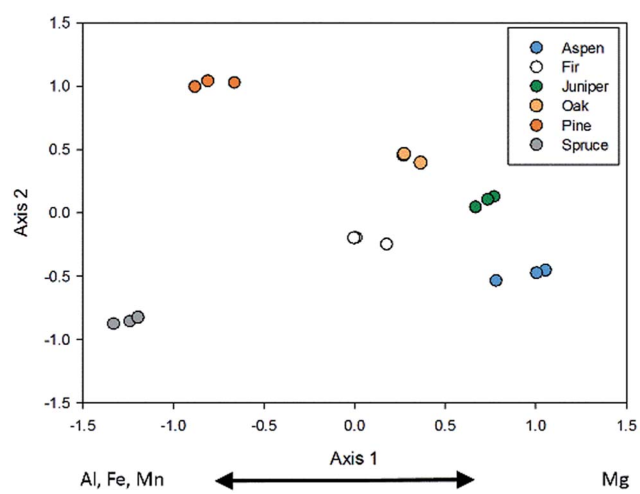


Fig. 2 Nonmetric multidimensional scaling ordination plot of total elemental concentrations in six tree species (taxa in legend, $n$ = 3), based on Bray–Curtis dissimilarities (stress = 0.01). The arrow direction indicates increased concentrations of elements.

and spruce. The SEM micrographs from all three tree species reveal the presence of square and rod morphologies in the ash surface, indicating the possible presence of crystalline solid phases. Additionally, these micrographs also show the presence of pores and different morphologic irregularities in the ash surfaces. All of these features illustrate the complexity in the morphology of ash surfaces. These features contribute to increased surface area and reactivity of ash in interfacial reactions with water. For example, a previous study reported that ash combustion can cause the formation of carbonate crystals and micro-pores in wildfire ash.[27]

The qualitative differences in elemental composition observed by EDX analyses in ash from these trees present similar characteristics to those observed in the previous subsection for the acid digestion results. For example, the concentrations of Al, Fe, and Mn are high in ash from pine and spruce in the EDX spectra, while they are below detection in ash from aspen. The added value of the SEM/EDX information compared to the acid digestion results is that the EDX elemental analyses correspond to a depth of approximately the top 1 μm of ash solid. Thus, the elements identified in these analyses at the ash surface could be key factors in interfacial reactions between ash and water.

We performed XPS analyses to further evaluate the chemical composition of the "near surface" (top 5–10 nm) region of ash solids. In addition to the identification of O 1s, C 1s and K 2s for all ash samples, XPS identified signals for Ca 2p, Mg 2p, Co 2p, Zn 2p, P 2p and S 2p in all ash samples (Table 2 and Fig. 4). The presence of Si 2p was identified in spruce and pine in a much larger content than in aspen. Consistent with EDX results, Al was not detected in aspen by XPS analyses. However, aspen has the largest content of Ca and Zn.

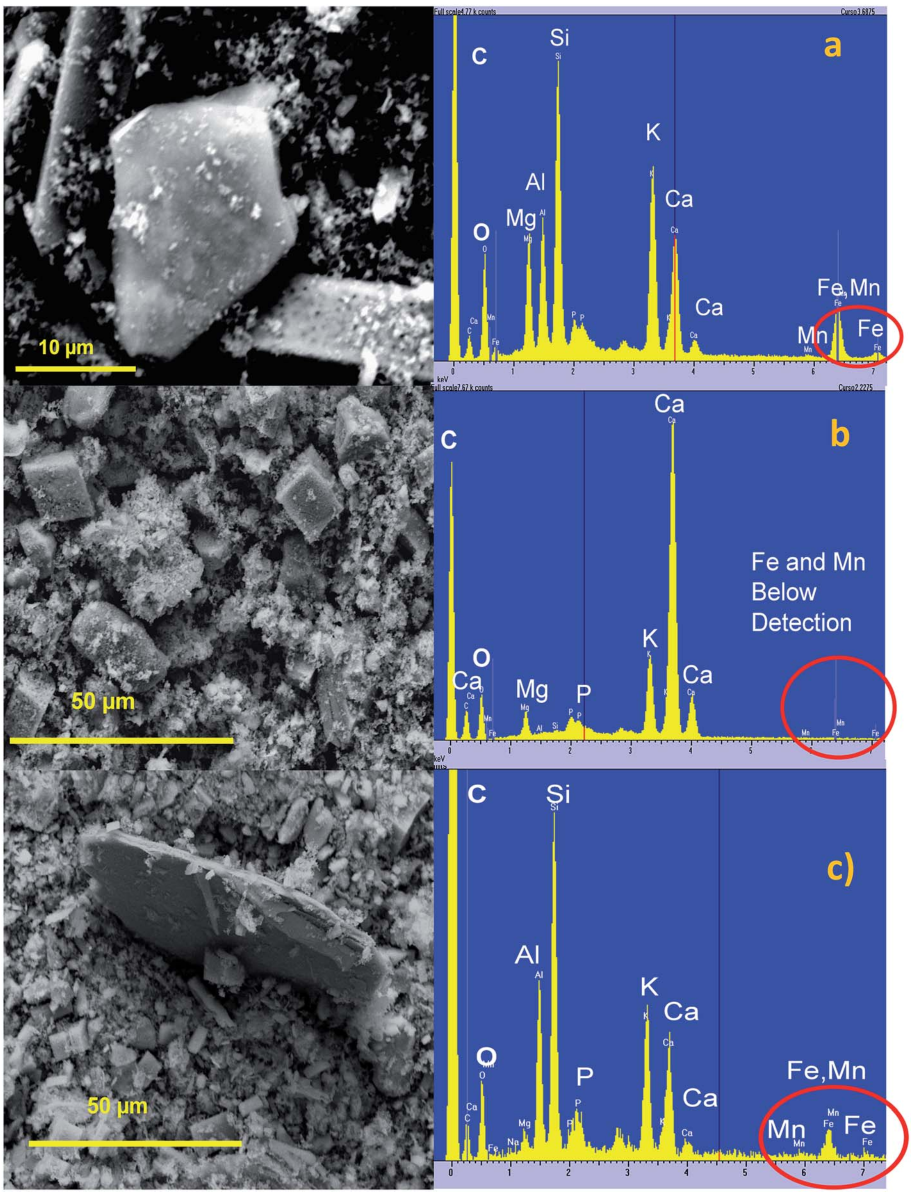


Fig. 3 SEM micrographs and EDX spectra of ash from: (a) pine; (b) aspen; and (c) spruce. The red circles highlight peaks specific for Fe and Mn.

Table 2 Survey XPS atomic composition of ash samples

| Atomic% | | | | | |
|---|---|---|---|---|---|
| Sample | Ca 2p | Mg 2p | Al 2p | Fe 2p | Mn 2p |
| Pine | 6.45 | 5.91 | 0.37 | | |
| Aspen | 9.06 | 6.63 | | | |
| Spruce | 7.35 | 2.88 | 0.84 | 0.23 | 0.64 |
| Sample | Si 2p | Zn 2p | Co 3p | P 2p | S 2p |
| Pine | 4.19 | 0.08 | 0.08 | 2.33 | 0.32 |
| Aspen | 0.58 | 0.25 | 0.20 | 0.97 | 0.15 |
| Spruce | 9.57 | 0.05 | 0.16 | 1.92 | 0.42 |

Low concentrations (less than 0.7 atomic percent) of Fe and Mn were detected only in ash from spruce by XPS. The P 2p peak at ∼134 eV, which is characteristic of phosphate,[35,36] and the S 2p peak at 168.3 eV, which is characteristic of sulfate,[37] were identified for all trees. Additional analyses were performed to further identify specific crystalline phases and bulk elemental content in wood ash samples.

### 3.3. X-ray diffraction (XRD) and micro-X-ray fluorescence (μ-XRF) analyses

Metal-bearing carbonate and oxide solid phases were identified in ash from pine, aspen, and spruce. Although some similarities were observed, unique mineralogical features were detected in ash from each tree species. The XRD patterns (Fig. 5a) and quantitative results of the peaks (Table S3†) suggest that the content of amorphous phases in the ash samples from the pine, aspen, and spruce are different. Interestingly, the quartz content in ash from aspen was very low, as was its amorphous phase content. However, the pine had the highest content of amorphous phase. This result suggests that it is possible that $SiO_2$ (am) is the main phase contributing to the amorphous signal in all samples. Common phases that were observed in all ash species are quartz [$SiO_2$], calcite, dolomite [$(Ca,Mg)CO_3$], fairchildite [$K_2Ca(CO_3)_2$], and kutnohorite [$Ca_{1.11}Mn_{0.89}(CO_3)_2$]. The mineral magnesite ($MgCO_3$) is likely present in ponderosa ash, while a spinel phase similar to magnetite ($Fe_3O_4$) was observed in aspen ash. Microcline ($K_{0.85}Na_{0.15}AlSi_3O_8$) was found in ponderosa ash while albite was found in spruce ash. Other studies have determined that ash is composed of silicates, oxides, phosphates, carbonates, sulfates, and amorphous phases that are either primary minerals in plant materials or undergo structural alterations from the heating during fire combustion.[23–26] Minerals such as calcite, quartz, and feldspar have been reported as predominant minerals in ponderosa pine ash.[32]

The XRD patterns of the soils at locations where pine, aspen, and spruce samples were collected are presented in Fig. 5b. These results indicate that the mineralogical composition of the

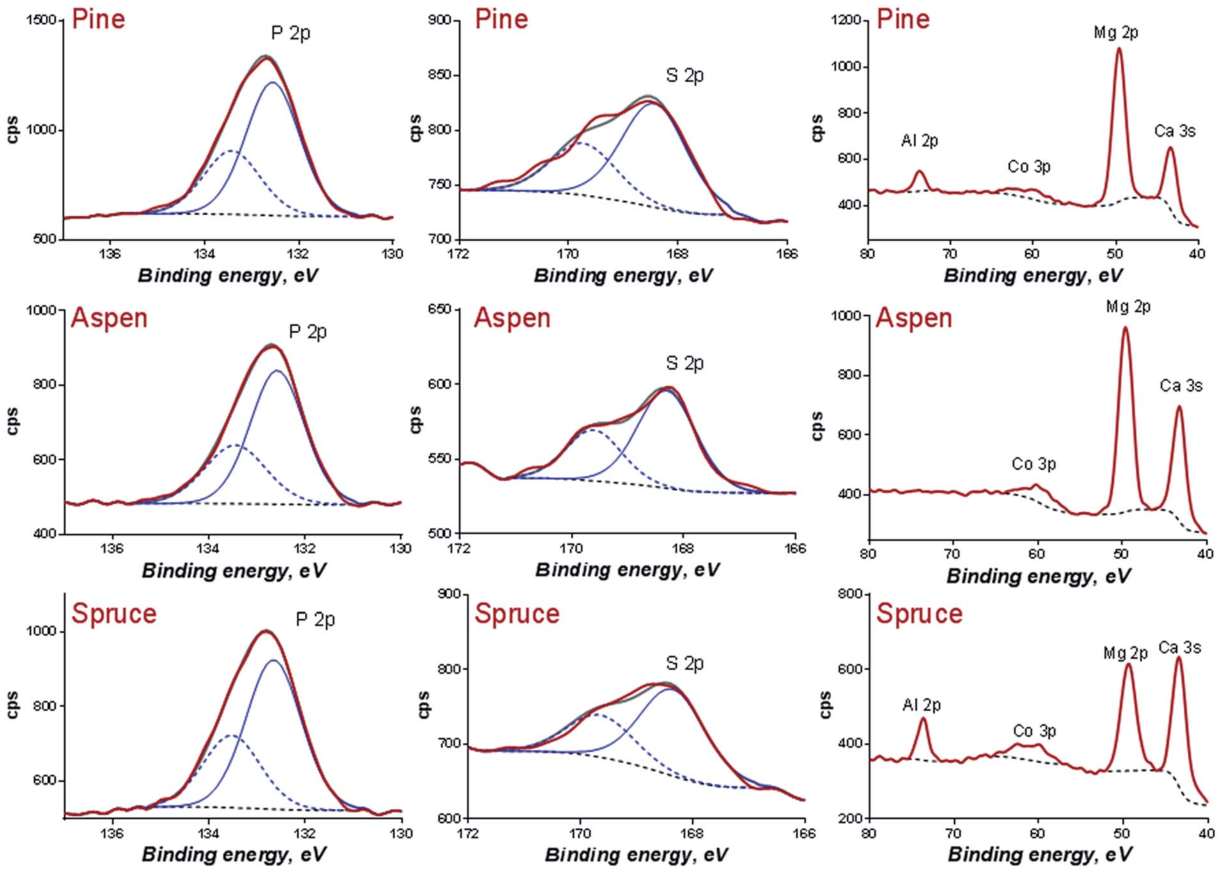


Fig. 4 High resolution XPS spectra of ash from pine, aspen, and spruce.

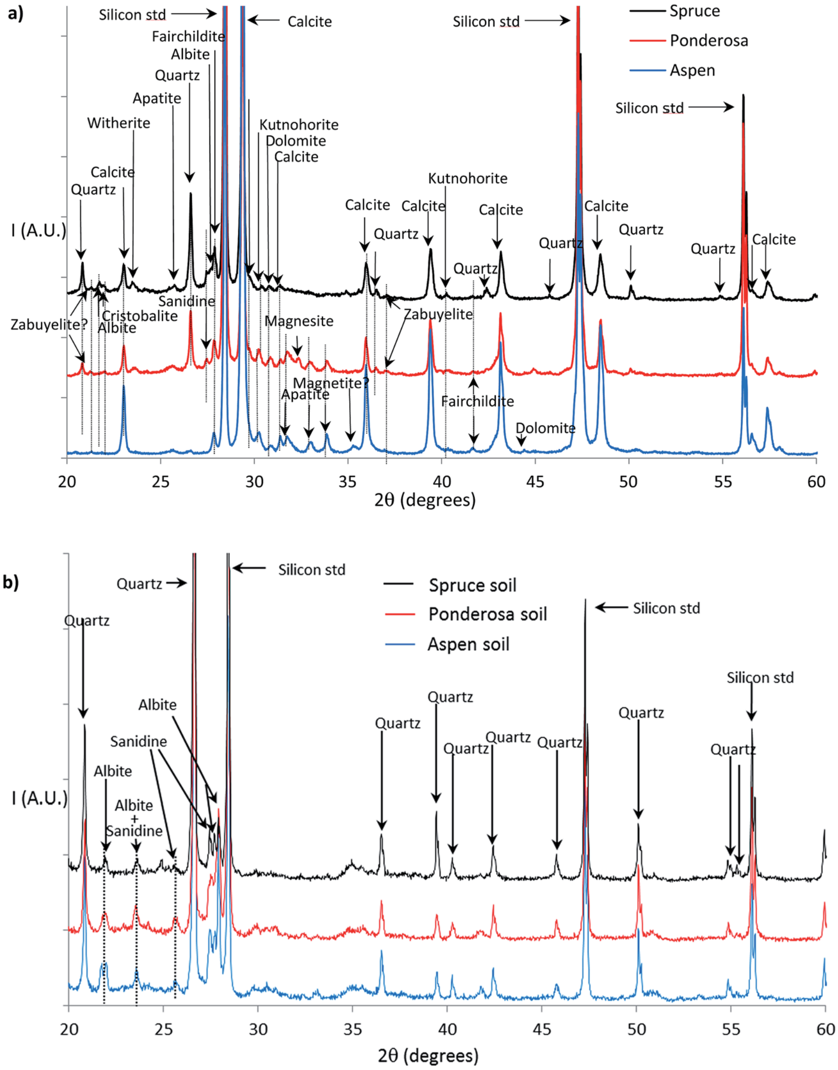


Fig. 5 XRD patterns of: (a) ash from pine, spruce, and aspen; and (b) soils from locations where pine, spruce, and aspen were collected.

soils is very similar for all samples. However, the mineralogical composition of the soil is different from the ash. The most predominant phases found in the soils were quartz and feldspar. In contrast to the ash samples, the predominance of carbonate and oxide phases was not noticeable in the soils. Some mineral phases such as quartz and albite ($NaSi_3O_8$) are present in ash and soils from which pine, aspen, and spruce were collected. Future studies should investigate the correlation between minerals in soil *vs.* those observed in trees to identify the mechanisms of metal accumulation.

The results obtained from micro-XRF confirm the XRD, spectroscopy, and microscopy analyses presented in previous sections. XRD and XPS have identified the overall chemical and mineral-phase composition of ashes while micro-imaging XRF allows analysis of elemental distribution. Micro-XRF elemental analysis of ashes (shown in Fig. 6) indicates that all samples have high concentrations of Ca, Mg, K and P, coinciding with the characteristics of the acid digestion data presented above. The predominance of Ca detected by XRF is in good correspondence with an abundance of Ca-containing phases, such as calcite, dolomite, apatite and others shown in XRD. The elements Mn, Fe, S and Zn are less concentrated in all ash samples. Silicon is detected in small concentrations in aspen ash, consistent with the XRD results which suggest that aspen has the lowest content of amorphous phase [*e.g.*, likely $SiO_2$ (am)]. On the other hand, the highest concentrations of Si were detected in pine ash, consistent with the XRD analyses which suggested that ash from pine had the highest content of amorphous phase. Aspen also contains a small amount of palladium (Pd).

XRF images were acquired for all elements detected. Multivariate curve resolution was used to combine images that have a similar spatial distribution into smaller number of chemical maps. Three maps, each representing individual chemical components that are spatially differentiated from other chemical components, can be displayed as red, green and blue images (Fig. 6). The red channel component in images from all ashes shows spatial distribution of phosphates and sulfates of

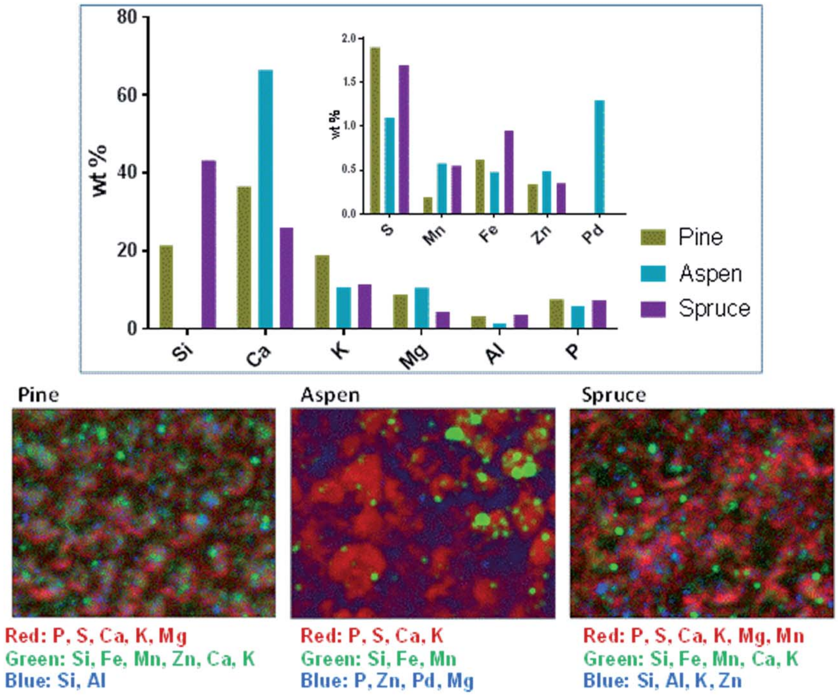


Fig. 6 Micro-XRF images of ash from pine, spruce, and aspen.

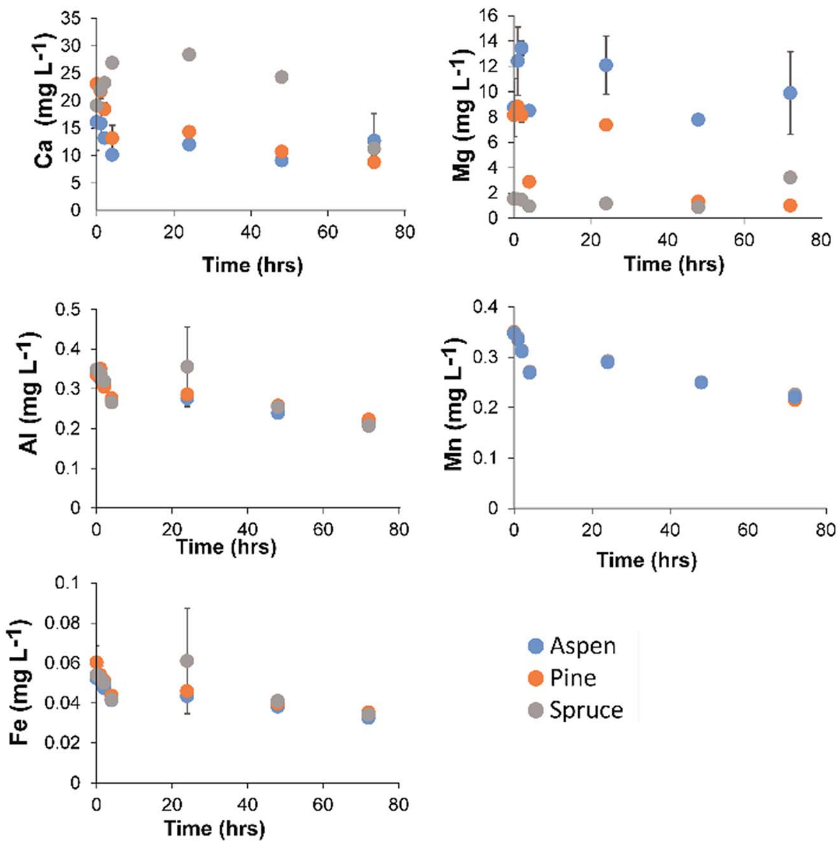


Fig. 7 Aqueous concentrations of Ca, Mg, Al, Mn, and Fe (in mg $L^{-1}$) over time measured for laboratory experiments after reacting ash with 18 MΩ water ($n = 3$).

Ca and K. The presence of phosphates and sulfates is confirmed by chemical speciation obtained by XPS, while apatite is detected by XRD. Ashes from spruce and pine have much smaller particulates of these phases that are more homogeneously distributed than in aspen.

The XRF map of aspen ash shows the highest concentrations of Ca and K, consistent with the identification of Ca- and K-containing mineral phases by XRD. Phosphates and/or sulfates of Mn and Mg could be present in spruce ash samples, consistent with the identification of kutnohorite [$Ca_{1.11}Mn_{0.89}(CO_3)_2$] by XRD.

The second major component is captured as a green channel in images, showing the distribution of silicates. Silicates of Ca, K, Fe and Mn are homogeneously distributed as small particles in the ash of pine and spruce, while in aspen ash only individual larger grains of Fe and Mn silicates are observed in smaller concentrations. In aspen ash, Ca and K are present as phosphates and sulfates and not as silicates, while in pine and spruce ash, both types of salts of Ca and K are detected. A correlation between Zn and silicate was detected in pine ash.

The third component is captured by the blue channel in RGB images, which is the major component that differentiates the ashes from each other. In pine, mostly Al-silicates are present as small scattered grains. Micro-XRF is able to differentiate between mixed silicates (green channel) and Al silicates (blue channel), which are separated laterally in pine ash. In spruce ash, silicates of Al, Zn and K are also present as small scattered particles. In aspen ash, which had the largest concentration of Mg, Zn and Pd, the phosphates of these elements are present as homogeneously distributed background phases.

Given that the mineralogy of different phases present in ash was determined, the effect of interfacial reactions of metals associated with ash solids on water chemistry was further explored through laboratory experiments.

### 3.4. Laboratory experiments

**3.4.1 Reactivity of Ca, Mg, Al, Fe, and Mn.** Metals were released in the initial sample of the batch laboratory experiment after reacting ash from pine, aspen, and spruce with 18 MΩ water and 10 mM $HCO_3^-$ solutions (Fig. 7 and 8). The release of these metals is likely due to the reactivity of metals in ash present as weakly bound and/or easily dissolvable metal-bearing carbonate or oxide solid phases (as identified by X-ray diffraction analyses). The concentrations of Ca and Mg released to solution vary for different species likely due to the different mineralogy of the ash from these trees. The high concentrations of Ca and Mg released from experiments reacted with ash from aspen in the laboratory batch experiments are consistent with the XPS data, indicating that aspen ash had the highest concentration of Ca and Mg at the surface and therefore was likely more susceptible to interfacial reactions. However, the

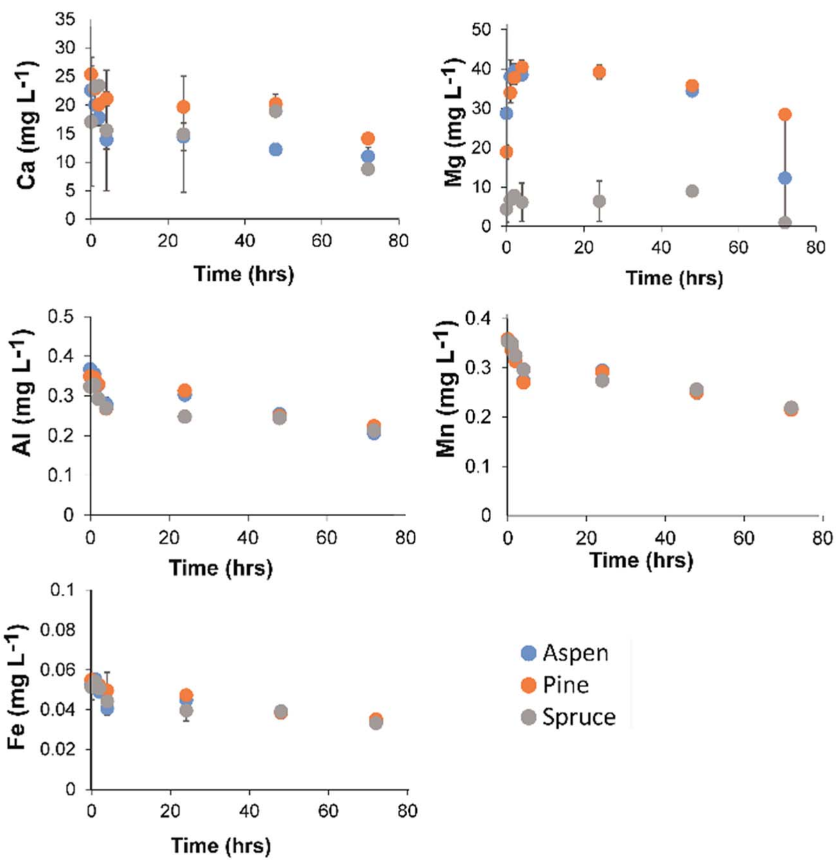


Fig. 8 Aqueous concentrations of Ca, Mg, Al, Mn, and Fe (in mg $L^{-1}$) over time measured for laboratory experiments after reacting ash with 10 mM $HCO_3^-$ ($n = 3$).

 

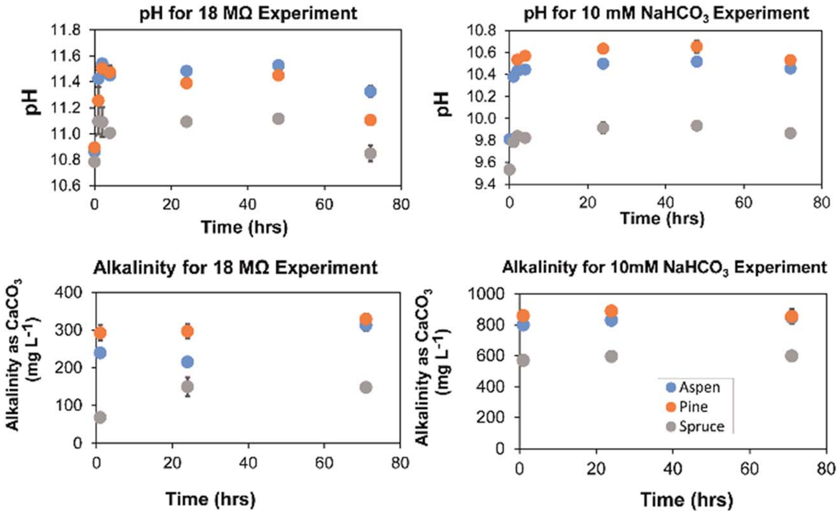


Fig. 9 pH and alkalinity ($CaCO_3^-$ mg $L^{-1}$) from laboratory experiments after reacting ash with 18 MΩ water and 10 mM $HCO_3^-$ ($n = 3$).

concentrations of these metals in all experiments decrease over time, suggesting that these metals can re-associate to ash solids due to adsorption.

The re-association of metals to ash over the course of the experiment can be explained by the adsorptive capacity of carbonate phases in ash. Metals such as Al, Mn, and Fe are released in the early stages of the experiment but their concentrations in solution decrease over time. The metals Al, Mn, Fe, and V have a higher adsorption affinity to metal-carbonate and metal-oxide phases in the ash compared to Ca and Mg, consistent with what has been reported in the literature.[38] The increase in sorptive properties of carbonate phases resulting from ash combustion has been reported in other studies.[27] The presence of carbonate crystal phases and micropores from ash combustion can increase ash porosity, water retention, and sorptivity.[27]

The dissolution of metal-carbonate phases caused an increase in solution pH in the initial times for experiments with 18 MΩ water and 10 mM $HCO_3^-$. As expected, the solution pH stabilized in the well-buffered experiments with 10 mM $HCO_3^-$ due to the buffering capacity of bicarbonate initially present in solution. It is also known that wood combustion produces alkaline ash; so, the dissolution of carbonate from carbonate minerals in ash can also cause an increase in water pH.[23,26,33] However, the solution pH decreased over time for experiments with 18 MΩ water (Fig. 9). Fluctuations in pH in non-buffered reactors are possibly due to the influence of aqueous metal hydroxide complexes (metals acting as Lewis acids) and decrease of $CO_3^{2-}$ as a function of solution pH due to exchange with the atmosphere (system to atmosphere). This effect could be relevant in waters with low levels of alkalinity such as storm runoff.

**3.4.2 Reactivity of anions and organic carbon.** A comparable release of sulfate and nitrate was observed for experiments performed with 18 MΩ and 10 mM $HCO_3^-$. However, phosphate concentrations are higher in the pine and spruce species compared to the aspen for the experiments with 10 mM $HCO_3^-$. Sulfate, nitrate, and phosphate data obtained for laboratory experiments are presented in the ESI (Fig. S1 and S2†). Pine has the highest concentrations of these three anions. The range of sulfate concentrations released from all tree species is 20 to 90 mg $L^{-1}$, and the range of nitrate concentrations released was 1 to 40 mg $L^{-1}$. The increase in nitrate and phosphate after pre-fire and post-fire storm events has been reported in the East Fork Jemez River.[15] The wood obtained for the ash investigated in this study was from a similar location (Fig. 1).

A limited release of dissolved organic carbon (DOC) in solution was observed for experiments performed with 18 MΩ and 10 mM $HCO_3^-$. The data for DOC concentrations obtained for laboratory experiments are presented in the ESI (Table S4†). Note that the DOC concentrations were lower than 1 mg $L^{-1}$ DOC. The burning conditions selected for this study, limited to 550 °C for 4 hours, led to organic matter loss as suggested by our data. However, a variety of mild, medium, and high fire severity and burn intensity scenarios can occur in catastrophic wildfire events.[28,29] Future research is necessary to understand the differences in chemical composition and effects of ash produced at lower and higher fire severity and burn intensity conditions than those selected for this study. A recent study of the characteristics of wildfire ash from Mediterranean conifer forests reported that organic matter decreases and inorganic carbon increases in wildfire ash with increasing combustion completeness.[39] For instance, at high combustion completeness, at temperatures higher than 450 °C, wood ash is composed mostly of inorganic carbonates; at temperatures higher than 580 °C, inorganic oxides are more predominant.[26]

## 4. Summary and conclusions

Knowledge about water quality effects caused by post-fire storms is essential to ensure the long-term recovery of watersheds from extreme catastrophic wildfire events. In this study, we identified differences in the chemical composition of six different tree species. The integration of microscopy, spectroscopy, and controlled laboratory conditions selected for this study enabled us to identify the presence of metals at the surface of wood ash, which are present as weakly bound and/or metal-bearing carbonate and oxide phases that are readily susceptible to react with 18 MΩ water and 10 mM $HCO_3^-$ solutions. The decrease in metal concentrations in solution over time observed in these laboratory experiments was likely due to adsorption of these metals onto the ash surface. It is also worth noting that although carbonate dissolved from ash can cause the water pH to increase, these metals can act as Lewis acids and cause the pH to decrease in waters that have low alkalinity and are not well buffered (*e.g.*, 18 MΩ water, storm water). However, in the experiments with 10 mM $HCO_3^-$ (equivalent to an alkalinity of 500 mg $L^{-1}$ as $CaCO_3$ which provided buffering capacity to the water), the pH increased at the early stages of the experiment due to the dissolution of carbonate phases in ash, but remained more stable over time. These results have important implications to better understand the increase in metal concentrations after post-fire storm events in water sources that have low alkalinity, such as storm water, and those waters with high alkalinity such as those sourced in carbonate lithologies.

Although the controlled laboratory conditions selected for this study helped us learn about the reactivity of metals in wood ash in this first stage of the investigation, the authors acknowledge the limitations of the experimental conditions selected. For example, the laboratory experiments from the current study were performed under batch conditions with adequate mixing time for adsorption to occur. However, these conditions are not representative of the dynamic interactions occurring when storm runoff transports ash and other sediments under surficial conditions. This study provided the ability to isolate the impact of ash contributions of tree species to water quality. A goal of future work is to better understand the influence of soil chemistry on ash composition to predict how species variation across a landscape impacts water quality post-fire under different fire severity and burn intensity scenarios. It is also important to consider the effect of redox-active metals such as Fe and Mn on dissolved oxygen concentrations, and reactive transport and interactions among ash, sediments, and water. Future studies are needed to adequately investigate these dynamic interactions under more realistic flow and environmental conditions.

## Acknowledgements

The authors thank Dr Robert Parmenter and Mark Ward (VCNP) for initial material and scientific advice for the sampling locations and other aspects of this study. The authors appreciate the contributions of Natalie Correa, Eliane Hayek, Asifur Rahman, and Cyrena Ridgeway (assistance with laboratory experiments), and Michael Spilde (SEM analyses). Dr Cliff N. Dahm provided invaluable advice, ideas, and encouragement to develop this investigation. Funding for this research was provided by the Oak Ridge Associated Universities (ORAU) Program Ralph E. Powe Jr Junior Faculty Enhancement Award, the New Mexico Water Resources Research Institute, and the National Science Foundation under New Mexico EPSCoR (Grant Number #IIA-1301346), and CREST (Grant Number 1345169). Any opinions, findings, and conclusions or recommendations expressed in this publication are those of the author(s) and do not necessarily reflect the views of the National Science Foundation.

## References

1 A. Abdelouas, W. Lutze and H. E. Nuttall, *Rev. Mineral.*, 1999, **38**, 433–473.
2 S. J. Pyne, P. L. Andrews and R. D. Laven, *Introduction to wildland fire*, John Wiley and Sons, 1996.
3 R. E. Keane, J. K. Agee, P. Fulé, J. E. Keeley, C. Key, S. G. Kitchen, R. Miller and L. A. Schulte, *Int. J. Wildland Fire*, 2009, **17**, 696–712.
4 N. Knowles, M. D. Dettinger and D. R. Cayan, *J. Clim.*, 2006, **19**, 4545–4559.
5 R. Seager, A. Tzanova and J. Nakamura, *J. Clim.*, 2009, **22**, 5021–5045.
6 A. P. Williams, C. D. Allen, A. K. Macalady, D. Griffin, C. A. Woodhouse, D. M. Meko, T. W. Swetnam, S. A. Rauscher, R. Seager and H. D. Grissino-Mayer, *Nat. Clim. Change*, 2013, **3**, 292–297.
7 P. J. Van Mantgem, N. L. Stephenson, J. C. Byrne, L. D. Daniels, J. F. Franklin, P. Z. Fulé, M. E. Harmon, A. J. Larson, J. M. Smith and A. H. Taylor, *Science*, 2009, **323**, 521–524.
8 P. J. Fawcett, J. P. Werne, R. S. Anderson, J. M. Heikoop, E. T. Brown, M. A. Berke, S. J. Smith, F. Goff, L. Donohoo-Hurley and L. M. Cisneros-Dozal, *Nature*, 2011, **470**, 518–521.
9 R. J. Bixby, S. D. Cooper, R. E. Gresswell, L. E. Brown, C. N. Dahm and K. A. Dwire, *Freshwat. Sci.*, 2015, **34**, 1340.
10 M. A. Wright, H. E. Mahowald and J. E. Payne, *Fiscal Year 2011 Actions Taken in Response to the Las Conchas Fire* at Los Alamos National Laboratory Environmental Protection Division, Los Alamos, New Mexico, 2012.
11 R. R. Parmenter, R. W. Oertel, T. S. Compton, S. Kindschuh, M. Peyton, W. Meyer, C. Caldwell, G. Z. Jacobi, O. Myers and M. Zeigler, Fire and floods in the Valles Caldera National Preserve, New Mexico: The 2011 Las Conchas Fire impacts on montane species diversity and food webs, Portland, OR, 2012.
12 A. C. Tillery, M. J. Darr, S. H. Cannon and J. A. Michael, *US Geological Survey Open-File Report*, 2011, p. 1308.
13 C. N. Dahm, R. I. Candelaria-Ley, C. S. Reale, J. K. Reale and D. J. Van Horn, *Freshwater Biol.*, 2015, **60**, 2584–2599.
14 J. K. Reale, D. J. Van Horn, K. E. Condon and C. N. Dahm, *Freshwat. Sci.*, 2015, **34**, 1426–1442.
15 L. R. Sherson, D. J. Van Horn, J. D. Gomez-Velez, L. J. Crossey and C. N. Dahm, *Hydrol. Processes*, 2015, **29**, 3193–3207.
16 P. Pereira and X. Úbeda, *J Environ Eng Landsc Manag*, 2010, **18**, 13–22.
17 P. Pereira, X. Úbeda and D. A. Martin, *Geoderma*, 2012, **191**, 105–114.
18 H. G. Smith, G. J. Sheridan, P. N. Lane, P. Nyman and S. Haydon, *J. Hydrol.*, 2011, **396**, 170–192.
19 E. D. Stein, J. S. Brown, T. S. Hogue, M. P. Burke and A. Kinoshita, *Environ. Toxicol. Chem.*, 2012, **31**, 2625–2638.
20 M. P. Burke, T. S. Hogue, A. M. Kinoshita, J. Barco, C. Wessel and E. D. Stein, *Environ. Monit. Assess.*, 2013, **185**, 10131–10145.

21 K. O. Odigie and A. R. Flegal, *PloS one*, 2014, **9**, e107835.
22 B. B. Gallaher, R. Koch and K. Mullen, Quality of storm water runoff at Los Alamos National Laboratory in 2000 with emphasis on the impact of the Cerro Grande Fire, Los Alamos National Laboratory LA-13926, 2002, p. 166.
23 A. Ulery, R. Graham and C. Amrhein, *Soil Sci.*, 1993, **156**, 358–364.
24 J. Quintana, V. Cala, A. M. Moreno and J. Parra, *J. Arid Environ.*, 2007, **71**, 45–56.
25 S. V. Vassilev, D. Baxter, L. K. Andersen and C. G. Vassileva, *Fuel*, 2010, **89**, 913–933.
26 M. B. Bodí, D. A. Martin, V. N. Balfour, C. Santín, S. H. Doerr, P. Pereira, A. Cerdà and J. Mataix-Solera, *Earth-Sci. Rev.*, 2014, **130**, 103–127.
27 V. N. Balfour and S. W. Woods, *Catena*, 2013, **111**, 9–24.
28 J. E. Keeley, *Int. J. Wildland Fire*, 2009, **18**, 116–126.
29 A. Parson, P. R. Robichaud, S. A. Lewis, C. Napper and J. T. Clark, *Field guide for mapping post-fire soil burn severity*, 2010.
30 R. Wetzel and G. Likens, *Limnological analysis*, Springer Science and Business Media, New York, 3rd edn, 2000.
31 B. McCune and M. J. Mefford, *PC-ORD, Multivariate Analysis of Ecological Data (V.5), MjM Software*, Gleneden Beach, Oregon, 2006.
32 E. J. Gabet and A. Bookter, *Int. J. Wildland Fire*, 2011, **20**, 443–452.
33 L. Etiegni and A. Campbell, *Bioresour. Technol.*, 1991, **37**, 173–178.
34 A. Alriksson and H. M. Eriksson, *For. Ecol. Manage.*, 1998, **108**, 261–273.
35 B. Feng, J. Weng, B. Yang, S. Qu and X. Zhang, *Biomaterials*, 2004, **25**, 3421–3428.
36 L. Ma, J. Zhu, Y. Xi, R. Zhu, H. He, X. Liang and G. A. Ayoko, *RSC Adv.*, 2015, **5**, 77227–77234.
37 National Institute of Standards and Technology (NIST), *Standard Reference Database 20, Version 4.1*, 2013.
38 M. M. Benjamin, *Water chemistry*, Waveland Press, 2014.
39 P. Dlapa, M. B. Bodí, J. Mataix-Solera, A. Cerdà and S. H. Doerr, *Catena*, 2015, **135**, 369–376.

 